Neurosci. Bull. June, 2020, 36(6):570–584
https://doi.org/10.1007/s12264-020-00467-w

www.neurosci.cn
www.springer.com/12264

ORIGINAL ARTICLE

# Reversal of Social Recognition Deficit in Adult Mice with *MECP2* Duplication *via* Normalization of MeCP2 in the Medial Prefrontal Cortex

**Bin Yu[1,2] · Bo Yuan[1] · Jian-Kun Dai[1] · Tian-lin Cheng[1] · Sheng-Nan Xia[1,2] · Ling-Jie He[3] · Yi-Ting Yuan[1] · Yue-Fang Zhang[1] · Hua-Tai Xu[1] · Fu-Qiang Xu[4] · Zhi-Feng Liang[1] · Zi-Long Qiu[1]**

Received: 19 August 2019 / Accepted: 16 November 2019 / Published online: 7 March 2020


**Abstract** Methyl-CpG binding protein 2 (MeCP2) is a basic nuclear protein involved in the regulation of gene expression and microRNA processing. Duplication of *MECP2*-containing genomic segments causes *MECP2* duplication syndrome, a severe neurodevelopmental disorder characterized by intellectual disability, motor dysfunction, heightened anxiety, epilepsy, autistic phenotypes, and early death. Reversal of the abnormal phenotypes in adult mice with *MECP2* duplication (*MECP2*-TG) by normalizing the MeCP2 levels across the whole brain has been demonstrated. However, whether different brain areas or neural circuits contribute to different aspects of the behavioral deficits is still unknown. Here, we found that *MECP2*-TG mice showed a significant social recognition deficit, and were prone to display aversive-like behaviors, including heightened anxiety-like behaviors and a fear generalization phenotype. In addition, reduced locomotor activity was observed in *MECP2*-TG mice. However, appetitive behaviors and learning and memory were comparable in *MECP2*-TG and wild-type mice. Functional magnetic resonance imaging illustrated that the differences between *MECP2*-TG and wild-type mice were mainly concentrated in brain areas regulating emotion and social behaviors. We used the CRISPR-Cas9 method to restore normal MeCP2 levels in the medial prefrontal cortex (mPFC) and bed nuclei of the stria terminalis (BST) of adult *MECP2*-TG mice, and found that normalization of MeCP2 levels in the mPFC but not in the BST reversed the social recognition deficit. These data indicate that the mPFC is responsible for the social recognition deficit in the transgenic mice, and provide new insight into potential therapies for *MECP2* duplication syndrome.

**Keywords** *MECP2* duplication · Medial prefrontal cortex · Social recognition deficit · CRISPR-Cas9

## Introduction

Methyl-CpG binding protein 2 (MeCP2) is a critical nuclear protein involved in transcriptional and post-transcriptional regulation [1–5]. Loss-of-function mutations in the *MECP2* gene have been found in 95% of patients with Rett syndrome, a devastating neurodevelopmental disorder with autistic phenotypes [6, 7]. Conversely, gain-of-function has also been identified in humans, typically through duplication or triplication of Xq28, which contains *MECP2* and defines another progressive neurological disorder, *MECP2* duplication syndrome, which shares core symptoms with autism spectrum disorder [8, 9].

*MECP2* duplication syndrome is a severe childhood neurodevelopmental disease that mainly affects males; it is characterized by profound mental retardation, poor speech

**Electronic supplementary material** The online version of this article (https://doi.org/10.1007/s12264-020-00467-w) contains supplementary material, which is available to authorized users.

✉ Zi-Long Qiu
zqiu@ion.ac.cn

1 Institute of Neuroscience, State Key Laboratory of Neuroscience, Chinese Academy of Sciences Center for Excellence in Brain Science and Intelligence Technology, Chinese Academy of Sciences, Shanghai 200031, China

2 University of Chinese Academy of Sciences, Beijing 100049, China

3 Department of Molecular and Human Genetics, Howard Hughes Medical Institute, Baylor College of Medicine, Houston, TX 77030, USA

4 Wuhan Institute of Physics and Mathematics, Chinese Academy of Sciences, Wuhan 430071, China

development, recurrent infections, epilepsy, motor dysfunction, anxiety, and autism [9, 10]. Transgenic mice that express a double or triple level of MeCP2 *via* insertion of the human *MECP2* gene (*MECP2*-TG) have been established, and recapitulate some of the symptoms in patients, including decreased motor activity, increased anxiety-like behaviors, seizures, and social deficits [11, 12]. Consistent with the clinical observations in humans, the phenotypes in mice that express a threefold dose of MeCP2 are much more severe [11, 13]. Interestingly, mice that overexpress the version of MeCP2 with mutations in either the methyl-CpG binding domain (MBD) or the transcriptional repression domain (TRD) are indistinguishable from wild-type littermates, indicating that both the MBD and TRD are indispensable for double MeCP2 to be toxic [14]. The neuropathological mechanism underlying *MECP2* duplication syndrome is still elusive. Recent studies have demonstrated that the relative cell density and number across cortical layers are essentially identical in *MECP2*-TG mice and controls; however, the spine turnover rate of layer V pyramidal neurons and dendritic arborization are dramatically changed during development in the transgenic mice [15]. Moreover, synaptogenesis, dendritic complexity, and the excitatory synaptic response are enhanced in neurons with *MECP2* duplication [16, 17], and the synaptic plasticity and synchrony of hippocampal neurons are abnormally elevated in *MECP2*-TG mice [11, 18]. These lines of evidence strongly imply that overexpression of MeCP2 does not affect the survival of neurons, and synaptic defects and circuit malfunction are the main manifestations of *MECP2* duplication syndrome.

Understanding the neuropathological mechanism of *MECP2* duplication syndrome has just begun, and no good intervention is available in the clinic. It is noteworthy that reversal of phenotypes in adult symptomatic *MECP2*-TG mice by correction of MeCP2 levels across the whole brain has been demonstrated [19], indicating that the neuroanatomy may remain intact in this disorder, so that correction of the molecular dysfunction can restore healthy physiology. However, whether different brain areas or neural circuits contribute to diverse aspects of the behavioral deficits is still unknown. Here, we report that using CRISPR-Cas9 technology to normalize MeCP2 levels in the medial prefrontal cortex (mPFC), but not the bed nuclei of the stria terminalis (BST) can reverse the social recognition deficit in adult *MECP2*-TG mice.

## Materials and Methods

### Mice

Mice with *MECP2* duplication (Stock No: 008679) on a pure FVB/N background were obtained from The Jackson Laboratory [11]. To bypass the issue of probable behavioral defects due to the premature retinal degeneration that develops in the pure FVB/N background [20], we used F1 hybrid *MECP2*-TG mice (FVB/N × C57Bl/6) as previously reported [12] for all experiments.

Mice were maintained in a temperature-controlled, SPF-level facility on a 12-h light–dark cycle and with *ad libitum* access to food and water. Only male mice were used. All animal breeding and experimental procedures were approved by and complied with the guidelines of the Animal Advisory Committee at the Shanghai Institutes for Biological Sciences, Chinese Academy of Sciences.

### Behavioral Phenotyping

*MECP2*-TG mice and littermate controls (2–4 months old) were familiarized with an experimenter blinded to the genotype for 4 to 5 days before behavioral phenotyping. All behavioral tests were performed during the dark period. Mice were habituated in the test room for 1 h before each test and at least one day of recovery was allowed between assays.

*Open Field Test*

After habituation, each mouse was placed in the center of an open arena (40 × 40 × 40 $cm^3$), and its behavior was tracked for 30 min by a camera above the arena. General locomotor activity was automatically analyzed by Ethovision XT 11.5 software (Noldus Information Technology, Wageningen, Netherlands).

*Light/Dark Box Test*

After habituation, each mouse was placed on the dark side (15 × 27 × 30 $cm^3$) of the light/dark box; this was connected to the light side (30 × 27 × 30 $cm^3$) by a small hole. Recording was performed by the overhead camera for 10 min. The time and frequency of mouse entries to the light side were recorded and analyzed by Ethovision XT 11.5 software.

*Elevated Plus Maze*

After habituation, each mouse was placed in the center of a plus maze consisting of two open arms (6 × 30 $cm^2$) and two closed arms (6 × 30 × 20 $cm^3$) 50 cm above ground. The time spent in the open arms was recorded for 10 min. Data analysis was performed by Ethovision XT 11.5 software.

*Three-Chamber Test*

This test was performed as previously described [21] with a few modifications. Age-matched C57BL/6 males were used as partner mice. Two days before the test, partner mice were placed randomly in either the left or right wire cage of the three chambers ($60 \times 40 \times 30$ $cm^3$) to habituate for 1 h per day. After habituation on the day of testing, the test mouse was first placed in the center of the three-chamber apparatus for the side-preference test. The time spent in exploring each wire cage was measured for 10 min. Next, during the social approach test, the partner mouse and a toy mouse was assigned to either the left or right cage in a counterbalanced manner. The amount of time the test animal spent in investigating the partner mouse or the toy mouse was measured for 10 min. Lastly, during the social novelty test, the toy mouse was replaced by a novel partner mouse and the partner mouse during the social approach test became the familiar partner mouse. The amount of time test animals spent investigating the familiar or novel partner mouse was measured for 10 min. All data were analyzed by Ethovision XT 11.5 software.

*Fear Conditioning Test*

Test animals were submitted to an auditory fear conditioning paradigm. Two different contexts, for conditioning (context A) and cued memory testing (context B), were used and the experiment lasted for three days. Freezing behavior was quantified by video-based software (FreezeFrame, Actimetrics Software, Wilmette, IL). In brief, each mouse was placed in context A to habituate for 10 min on the first day. Twenty-four hours after habituation, the mouse was subjected to fear conditioning sessions. The 4 min prior to the first conditioned stimulus (CS) (5 kHz, 90 dB, 20 s) were used to measure baseline freezing. The CS was paired to the unconditioned stimulus (US) (2 s, 0.5 mA footshock back to back with the last CS) and 5 CS/US pairings were presented in each conditioning session with an 80-s inter-trial interval. Twenty-four hours after conditioning, the mouse was tested for contextual fear memory in context A for 5 min. For the cued fear memory test, each mouse was placed in context B to habituate for 3 min, then the CS was presented and lasted for 3 min. The interval between the two tests in the same mouse was not less than 30 min. The percentage freezing in the first 3 min (in a new context) represented the extent of fear generalization, and the percentage freezing in the last 3 min reflected the cued fear memory.

*Novel Object Recognition Test*

This test lasted for three days. On the first day, each mouse was put into the apparatus (40 cm × 40 cm × 40 cm) to acclimate to the environment for 10 min after habituation in the test room. On day 2, two identical objects (blue cones) were placed on the same side of the apparatus, and the mouse was put into the apparatus to explore for 10 min. On day 3, all the processes were the same as on day 2, except that one of the old objects was randomly replaced with a new different object (a yellow cylinder). The exploration time was counted as the period for which mouse's nose entered the designated area 2 cm around the object. All data were analyzed by Ethovision XT 11.5 software.

*Sucrose Preference Test*

The tested mice, one per cage, were presented with two drinking bottles. Prior to the test, each mouse was habituated in their home cage for at least 3 days. After the acclimatization, the water in one bottle was replaced by 0.5% sucrose solution. Water and sucrose solution intake were measured daily for 4 days by weighing the bottles. The positions of the bottles were switched daily to reduce side bias. Mice were again presented with two bottles of water after the 0.5% sucrose preference test for 1 week. Then, the 2% sucrose preference test was performed using the same cohorts. All the procedures were the same as for the 0.5% sucrose preference test, except that the concentration of sucrose was 2%. Sucrose preference was calculated as the percentage of the volume of sucrose intake over the total volume of fluid intake and averaged over the 4 days of testing.

*Cocaine Conditioned Place Preference (CPP) Test*

The CPP boxes consisted of three compartments (16.8 cm × 12.7 cm × 12.7 cm for the left and right compartments and 7.2 cm × 12.7 cm × 12 cm for the central compartment). The right compartment was painted white and had a steel mesh floor, the left was painted black and had a steel rod floor, and the central compartment had gray walls and a smooth floor as a neutral zone. The test lasted for 11 days. On day 1, each mouse was put into the central compartment to freely explore the three compartments for 20 min for habituation. On day 2, the times each mouse spent in the black and the white compartments were recorded for 20 min with Anilab software. The less preferred compartment was used as the conditioned compartment, and the other was regarded as the unconditioned compartment. On day 3, the mouse received a cocaine injection (20 mg/kg) and was confined for 30 min in the conditioned compartment determined by the test on day 2. On day 4, the mouse received a saline injection paired with the unconditioned compartment for 30 min. Four drug sessions and four saline sessions were administered, and the last day of treatment was with saline. On the day of testing, day 11, the mouse received a saline injection, and the time spent in the black and white compartments was recorded for 20 min with Anilab software. The cocaine CPP score was calculated as the time spent in the conditioned compartment minus the time spent in the unconditioned compartment.

*Barnes Maze Test*

This test lasted for 13 days. Each day, experiments began after habituation for 1 h in the test room (strong light was applied to increase the motivation of mice to escape from the circular platform). Day 1 was for adaptation; each mouse was placed in a cylindrical black start chamber in the middle of the maze. Ten seconds later, the chamber was lifted and the mouse guided to the escape box. The mouse was allowed to stay in the box after covering with a lid for a dark reward for 2 min. On day 2, the mouse was placed in the middle of the maze as on day 1 and allowed to explore the maze for 3 min. The trial ended when the mouse entered the escape box or after 3 min had elapsed. The box was covered with a lid immediately after the mouse entered, and it was allowed to stay there for 1 min. If the mouse did not reach the goal within 3 min, the experimenter guided the mouse gently to the escape box and left it inside for 1 min. Mice received 4 trials per day with an inter-trial interval of 15 min for 4 days. During the training (days 2–5), the time to find and enter the escape box was measured manually. On day 6, 24 h after the last training day, the target hole was closed and short-term memory was tested. Mice were placed in the middle of the maze and allowed to explore for 90 s. The time to find the right target hole was measured manually. Long-term memory was assessed on day 13, using the same process as on day 6.

## MRI Data Acquisition and Data Processing

All imaging was performed on a 9.4 T/30 cm Bruker BioSpec scanner (Bruker, Ettlingen, Germany) with a 20 mm-diameter volume coil for radiofrequency pulse transmission and a mouse cryoprobe surface coil for signal detection. To overcome significant echo-planar imaging (EPI) signal dropout deep in the brain caused by the aural cavity magnetic susceptibility artifact, we introduced a liquid-phase fluorocarbon into the middle ear before imaging [22]. During an imaging session, the body temperature was maintained at 37°C ± 0.5°C by combining a warm water pad and a hot-air blower with temperature feedback (SAII, Stony Brook, NY), and respiratory rate was monitored (Model 1025, SAII, Stony Brook, NY). A rapid acquisition relaxation enhancement (RARE) $T_2$-weighted sequence was selected to acquire 22 coronal slices of 0.4 mm thickness, which covered the whole mouse brain volume. The anatomical images were obtained with an in-plane resolution of 0.063 mm × 0.063 mm (matrix size 256 × 256 and field of view (FOV) 16 mm × 16 mm), repetition time (TR) 3200 ms, echo time (TE) 33 ms, RARE factor 8, and three averages. During imaging, the mice were anesthetized with 3% isoflurane (0.5 bar). Resting-state fMRI data were scanned using a gradient echo EPI sequence with the following parameters: TR 2500 ms; TE 12 ms; flip angle 75°; matrix size 100 × 100; FOV 16 mm × 16 mm; in-plane resolution 0.16 mm × 0.16 mm; slice thickness, 0.4 mm; 22 coronal slices. One hundred twenty EPI volumes were acquired in each run, and 6 runs were obtained for each session. During imaging, the mice were anesthetized with a combination of 0.5% isoflurane (0.5 bar) and dexmedetomidine (0.015 mg/kg per hour), and the respiratory rate was maintained at ~90 breaths/min.

All the functional images of each mouse were first time-sliced and then realigned for motion correction using SPM8 (Welcome Trust Centre for Neuroimaging, London, UK). For each mouse, the average of aligned functional volumes was rigidly co-registered to its anatomical image. The anatomical image from each mouse was subsequently non-linearly warped to the space of a high-resolution three-dimensional mouse brain atlas [23]. Then, all the functional images from each mouse were directly warped to the space of the atlas by concatenating the transformation from each registration step. All the registration processes were carried out using Advanced Neuroimaging Tools [24]. After registration, all functional images were pre-processed with steps for motion, white matter, and cerebrospinal fluid signal regression, de-trending, and 0.01–0.1 Hz band-pass filtering. After preprocessing, a regional homogeneity (ReHo) map was generated by calculating Kendall's coefficient of concordance of the time series of a given voxel with those of its nearest neighbors (26 voxels). The pre-processed data without band-pass filtering were used to generate fractional amplitude of low-frequency fluctuation (fALFF) maps by dividing the sum of the amplitude across 0.01 Hz–0.08 Hz with that across the entire frequency range, 0 Hz–0.25 Hz [25]. Both ReHo and fALFF calculations were carried out using the free software REST (Resting-State fMRI Data Analysis Toolkit V1.8, http://restfmri.net/forum/REST_V1.8). All the ReHo and fALFF maps were smoothed with a 0.4-mm full width at half maximum Gaussian kernel.

## AAV Preparation

To construct the pAAV-Guide vector, sgRNAs that specifically target exon 3 of the human *MECP2* gene were designed using CRISPR design tools (http://crispr.mit.edu/ and http://crispr.dfci.harvard.edu/SSC/). The sgRNAs were introduced into the vector PX458 (Addgene, Watertown, MA, no. 48138) and U6-sgRNA cassettes were amplified by PCR. Then, the U6-sgRNA cassettes were ligated with the vector pAAV-GFP (Addgene, no. 50465). The pAAV-spCas9 plasmid was obtained from Addgene (no. PX551). High titer AAV-Guide ($3.9 \times 10^{12}$ viral genomes (vg)/mL), AAV-spCas9 ($1.7 \times 10^{13}$ vg/mL), and AAV-GFP ($5 \times 10^{12}$ vg/mL) particles were produced by the Gene

Editing Core Facility in the Institute of Neuroscience, Chinese Academy of Sciences.

### Analysis of On-Target Gene Editing *In Vitro*

For *in vitro* assays, primary cortical neuron cultures were prepared from transgenic mice on embryonic day 15. Cells were plated on poly-D-lysine-coated 6-well plates (ThermoFisher Scientific, Waltham, MA). About $1 \times 10^{11}$ viruses (1:1 mixture of AAV-spCas9 and AAV-Guide) were incubated with $\sim 1 \times 10^{6}$ cells per well at 2 days *in vitro* (DIV). The cells were digested at DIV 6 and GFP-positive cells were collected by a flow cytometer (MoFlo XDP, Beckman Coulter, Brea, CA). DNA extracted from sorted cells was used as the PCR template with forward primer 5′-GCCTGCCTCTGCTCACTTGTTC-3′ and reverse primer 5′-CCCTGCCCTGTAGAGATAGGAG-3′. The PCR product was purified and ligated with T easy vector (Promega, Madison, WI). Ligated plasmids were transfected into competent *Escherichia coli* and single clones were picked for further sequencing analysis.

### Stereotactic Injection

Mice were anesthetized by intraperitoneal injection of pentobarbital sodium (100 mg/kg) and mounted in a stereotaxic apparatus (RWD, Shenzhen, China). Body temperature was maintained by a heating pad and ophthalmic ointment was applied to maintain eye lubrication. A craniotomy was performed according to approved procedures by the Animal Advisory Committee at the Shanghai Institutes for Biological Sciences, Chinese Academy of Sciences. The craniotomy window was made using a hand-held drill, and a glass micropipette filled with viruses suspended in mineral oil was used to reach the target brain areas. Injections of viruses were carried out via a stereotaxic injector (Stoelting, Wood Dale, IL). After each injection, the micropipette was held in place for 10 min before retraction to allow for diffusion of viruses. The incision was sutured and mice were allowed to recover on a heating blanket before returning to their home cage.

To normalize MeCP2 levels in the mPFC (anterior/posterior: 2.3 mm; mediolateral: ± 0.3 mm; dorsal/ventral: −2.0 mm), a 1:1 AAV mixture of AAV-spCas9 and AAV-Guide was injected bilaterally into the mPFC of *MECP2*-TG mice at a volume of 500 nL for each site. To normalize MeCP2 levels in the BST (anterior/posterior: 0.15 mm; mediolateral: ± 0.9 mm; dorsal/ventral: − 4.9 mm/− 4.25 mm), a 1:1 AAV mixture of AAV-spCas9 and AAV-Guide was injected bilaterally into the BST of *MECP2*-TG mice at a volume of 300 nL for each site. A 1:1 AAV mixture of AAV-spCas9 and AAV-GFP at the same volume was used as control. After 6 weeks of expression, behavioral phenotyping was performed.

### Immunofluorescent Staining

Mice were anesthetized with pentobarbital sodium and perfused transcardially with saline followed by 4% paraformaldehyde (PFA, Sigma-Aldrich, St. Louis, MO). The brain was extracted and post-fixed in 4% PFA overnight at 4°C, followed by cryoprotection in 30% sucrose in phosphate-buffered saline (PBS) at 4°C. Coronal sections were cut at 50 μm on a vibratome (CM1950, Leica, Wetzlar, Germany). The sections were blocked for 1 h at room temperature in PBST (0.3% Triton X-100) with 5% bovine serum albumin, fraction V, followed by incubation with primary antibodies at 4°C overnight and secondary antibodies at room temperature for 2 h. The primary antibodies used were rabbit anti-MeCP2 (1:1000, CST, Danvers, MA) which recognizes both human and mouse MeCP2, and goat anti-GFP (1:500, Abcam, Cambridge, MA). The secondary antibodies used were donkey anti-rabbit IgG-CF 555 (1:1000, Biotium, Fremont, CA) and donkey anti-goat IgG-CF 488 (1:1000, Biotium). DAPI (1:10000, Roche, Basel, Switzerland) was used to stain nuclei. Images were acquired on a Nikon TiE-A1 plus confocal microscope (Nikon, Tokyo, Japan) and an Olympus VS120 fluorescence microscope (Olympus, Tokyo, Japan). Fluorescence intensity was measured using ImageJ (Open Source Software from NIH, Bethesda, MD). In Fig. 4D, the fluorescence intensity was compared between the mPFC (gene editing area) and an adjacent cortical area.

### Western Blot Analysis

Individual mice were rapidly decapitated, and the brain was immediately extracted and placed in ice-cold PBS. The transduced mPFC was microdissected under a dissecting microscope, and transferred to a 1.5-mL centrifuge tube containing ice-cold RIPA buffer and protease inhibitors (Roche). The tissue was homogenized with an electric homogenizer, then the tube was left on an orbital shaker for 2 h at 4°C. The cell lysate was centrifuged for 20 min at 12,000 rpm at 4°C in a microcentrifuge. Supernatants were dissolved in SDS-PAGE sample buffer, and proteins were separated on 8% SDS-PAGE gels. The primary antibodies used were rabbit anti-MeCP2 (1:1000, CST) and mouse anti-GAPDH (1:5000, Sigma-Aldrich, St. Louis, MO). The secondary antibodies used were anti-rabbit and anti-mouse HRP antibodies (1:2000, Sigma-Aldrich). Blots were imaged with a GE Amersham Imager600 system (GE Healthcare, Chicago, IL), and quantified using ImageJ.

### Statistical Analysis

GraphPad Prism software was used for statistical significance tests. The number of animals used and the specific statistical tests used are described in the figure legends. SPSS Software (SPSS Inc., Chicago, IL) test showed that all data values appeared to be normally distributed.

## Results

### Behavioral Phenotyping of Adult *MECP2*-TG Mice

The *MECP2*-TG mice were on a pure FVB/N background at first [11], but mice on this background develop premature retinal degeneration, which can confuse the interpretation of some behavioral phenotypes [20]. To overcome this issue, previous studies have characterized F1 hybrid *MECP2*-TG mice (FVB/N × C57BL/6 or FVB/N × 129S6/SvEv), which have several phenotypes reminiscent of patients with *MECP2* duplication syndrome, including increased anxiety, reduced locomotor activity, and abnormal social behaviors [12]. Therefore, we used F1 hybrid *MECP2*-TG mice. First, we performed more extensive behavioral phenotyping of F1 hybrid *MECP2*-TG mice (FVB/N × C57BL/6), and found that they displayed decreased locomotor activity in the open field test, as previously described (Fig. 1D). In addition, transgenic mice were prone to manifest aversive-like behaviors, including a heightened anxiety and fear generalization phenotype. Compared to their wild-type littermates, *MECP2*-TG mice spent less time in the light compartment of the light–dark box and in the open arms of the elevated plus maze (Fig. 1E, F), which represented a robust anxiety phenotype in the *MECP2*-TG mice. In the fear conditioning test, *MECP2*-TG mice exhibited a remarkable increase of percentage freezing, whether in the training phase (Fig. 1G), the contextual and cued fear memory test phase (Fig. 1H, I), or when test mice were placed in a new context after training (Fig. 1J). It is worth noting that the baseline percentage freezing before the first trial was very low in both genotypes, and transgenic mice displayed an extremely high percentage freezing in the first trial. These data indicated that *MECP2*-TG mice have an excessive startle response and fear generalization phenotype. To investigate social behavior, we tested *MECP2*-TG mice in the three-chamber test for social approach and social novelty (Fig. 1A–C), and discovered that they had a deficit in social novelty behavior as revealed by an inability to distinguish a novel partner mouse from familiar partner mouse, but social approach behavior was basically normal, demonstrating that social recognition is impaired in *MECP2*-TG mice.

Because *MECP2*-TG mice presented elevated aversive-like behaviors, we hypothesized that their appetitive behaviors may be disturbed as well. Next, we sought to examine reward-related behaviors using the sucrose preference test and the cocaine CPP test. Surprisingly, *MECP2*-TG mice exhibited normal preference for 0.5% and 2% sugar water (Fig. 2A), and spent more time in the cocaine-conditioned chamber, consistent with wild-type littermates (Fig. 2B). There was no statistically significant difference in the performance between transgenic mice and littermate controls, indicating that reward-related behaviors are basically intact in *MECP2*-TG mice. Moreover, freezing behavior was dramatically enhanced in *MECP2*-TG mice, which may be due to increased learning and memory in the transgenic mice. We thus used a less stressful behavioral paradigm to explore learning and memory in *MECP2*-TG mice. In the novel object recognition test, both transgenic mice and their wild-type littermates showed normal preference for the novel object (Fig. 2C). And no difference was observed in the Barnes maze test between *MECP2*-TG mice and controls (Fig. 2D–F). These data suggested that learning and memory functions are not damaged in *MECP2*-TG mice, and the increased freezing behaviors in the fear conditioning test probably result from fear generalization.

### Resting-State fMRI Analysis of Adult *MECP2*-TG Mice

Although MeCP2 is ubiquitously expressed across the whole brain, another question to be addressed is whether all cell types are equally affected by doubling the MeCP2 levels or whether certain cell types or regions are more sensitive. Previous studies of conditional knockout of *Mecp2* in mouse brain have provided strong evidence that MeCP2 plays different roles and is not equally important in different cell types and areas [26–28]. In addition, our behavioral phenotyping results showed that appetitive behaviors and learning and memory were basically normal in *MECP2*-TG mice, implying that the regions or neural circuits associated with these behaviors are intact in *MECP2*-TG mice. To identify which areas or circuits are responsible for the abnormal behaviors, we used resting-state fMRI to scan the whole brain of *MECP2*-TG mice and wild-type controls. Because significant EPI signal is lost in deep brain areas due to the aural cavity magnetic susceptibility artifact, we introduced a liquid-phase fluorocarbon into the middle ear by needle puncture as previously reported. This method allowed us to acquire whole brain fMRI data without signal dropout [22]. Our imaging data manifested significant ReHo value differences in multiple areas between *MECP2*-TG and wild-type control mice (Fig. 3A, B). Importantly, differences were concentrated in

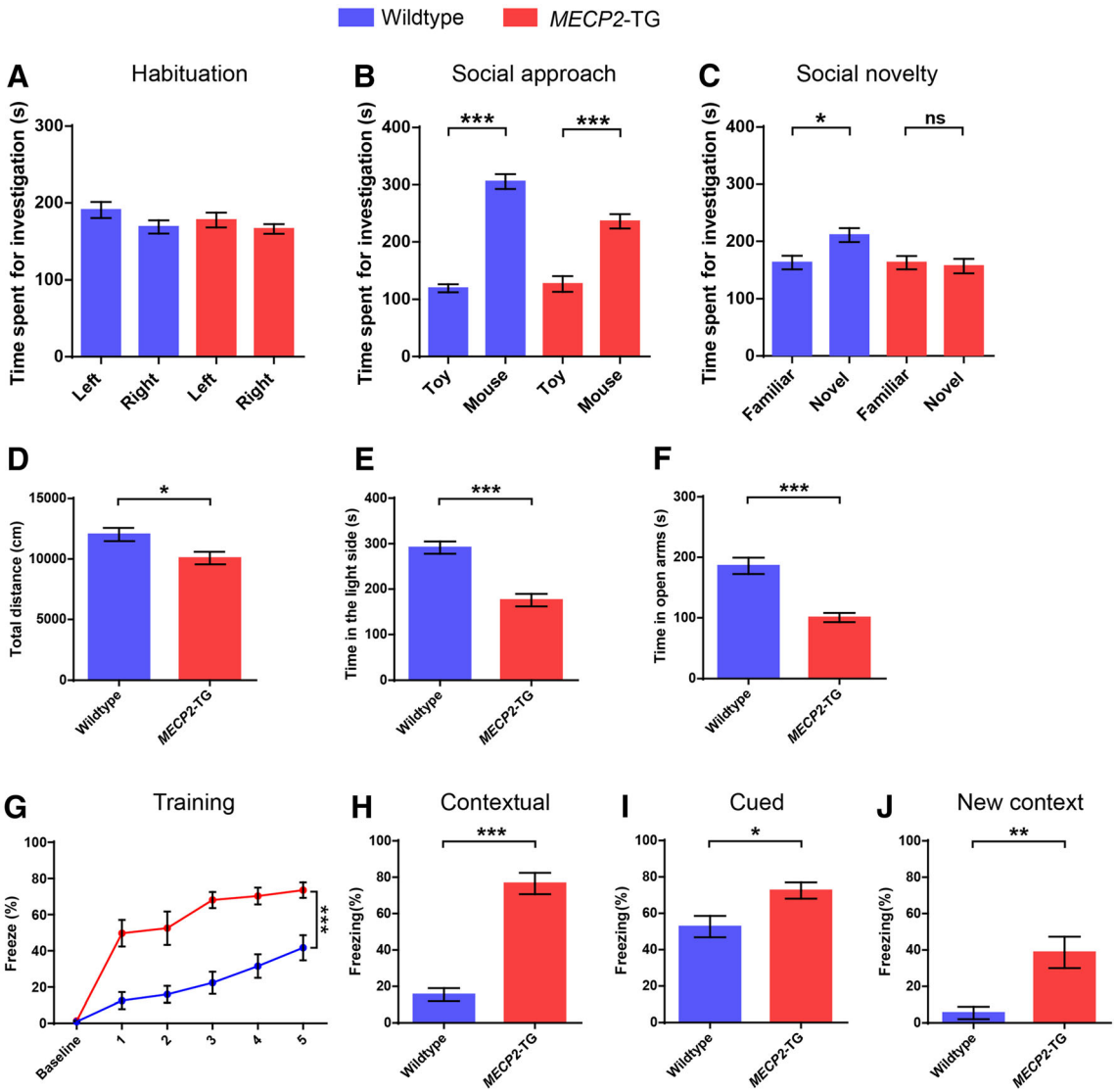


**Fig. 1** *MECP2*-TG mice display reduced locomotor activity, enhanced aversive behaviors, and a social recognition deficit. **A–C** *MECP2*-TG mice and wild-type littermates manifested no side preference (**A**) and normal social approach behavior (**B**), but *MECP2*-TG mice did not distinguish familiar partners from novel partners (**C**) as wild-type littermates did in the three-chamber test. **D** *MECP2*-TG mice travelled less in the open field than their wild-type littermates. **E, F** Compared to their wild-type littermates, *MECP2*-TG mice spent less time on the light side of the light/dark exploration box, and less time in the open arms of an elevated plus maze. **G–J** Percentage freezing was significantly higher in the *MECP2*-TG mice than in wild-type littermates during the training phase (**G**), the contextual fear memory testing phase (**H**), the cued fear memory testing phase (**I**), or when presented with a mouse in a new context after training (**J**). $n$ = 10–14 for wild-type, $n$ = 10–14 for *MECP2*-TG. Data are the mean ± SEM. ns, not significant. $^{*}P < 0.05$, $^{**}P < 0.01$, $^{***}P < 0.001$ (two-tailed paired $t$-test in **A–C**, two-tailed $t$-test in **D–F** and **H–J**, and two-way repeated-measures ANOVA in **G**).

areas modulating aversive behaviors, including the mPFC, BST, amygdala, hypothalamus (HY), thalamus, piriform area, anterior cingulate, and periaqueductal gray. Furthermore, we generated fALFF maps and found that the fALFF values showed differences consistent with the ReHo results in most areas (Fig. S1). These data were consistent with our behavioral results.

## Normalization of MeCP2 Levels in the mPFC Reverses the Social Recognition Deficit in Adult *MECP2*-TG Mice

Reversal of abnormal phenotypes in adult *MECP2*-TG mice by normalizing the MeCP2 levels across the whole brain has been demonstrated [19]. However, which brain areas or neural circuits have defects that contribute to disease phenotypes was not known. Accumulating

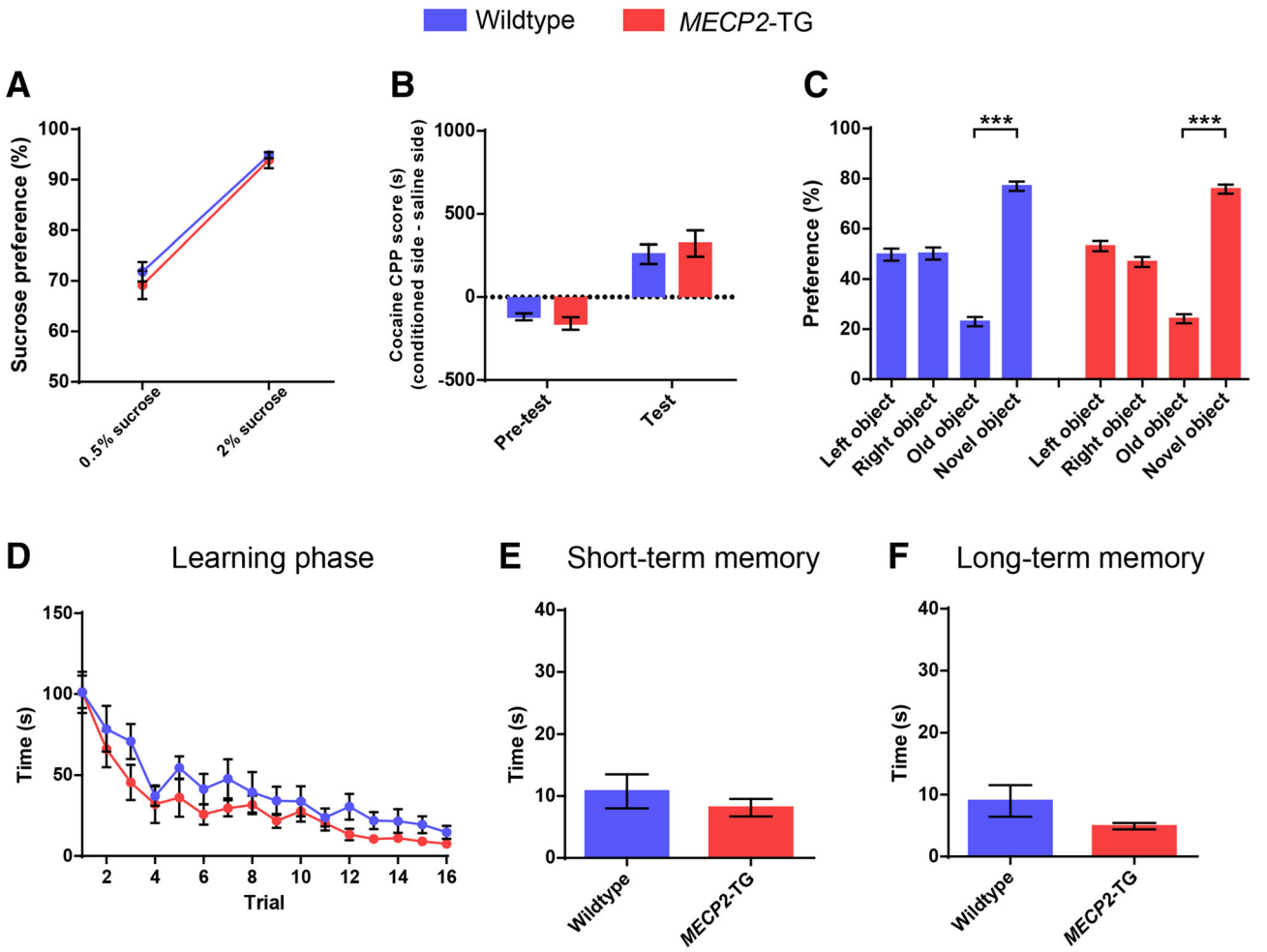


**Fig. 2** *MECP2*-TG mice display normal appetitive behaviors, novel object recognition, and spatial learning and memory. **A, B** *MECP2*-TG mice and wild-type littermates showed comparable sucrose preference (**A**), and cocaine conditioned place preference (**B**). **C** In the novel object recognition test, *MECP2*-TG mice and wild-type littermates showed no side preference during habituation, and normal preference for the novel object in the test phase. **D–F** No significant difference was found between *MECP2*-TG mice and wild-type littermates during the learning phase (**D**), the short-term memory test (**E**), and the long-term memory test (**F**) in the Barnes maze test. $n$ = 10–14 for wild-type, $n$ = 10–14 for *MECP2*-TG. Data represent the mean ± SEM. $^{***}P < 0.001$ (two-tailed $t$-test in **A, B, E,** and **F**, two-tailed paired $t$-test in **C**, and two-way repeated-measures ANOVA in **D**).

evidence has shown that the mPFC mediates social recognition behaviors, and its dysfunction leads to social recognition deficits [21, 29–32]. The mPFC was also one of the areas showing the most significant difference in ReHo value in our fMRI data (Fig. 3), so we reasoned that mPFC dysfunction is likely to underlie the social recognition deficit in *MECP2*-TG mice. To test the hypothesis, we used the CRISPR-Cas9 gene editing system similar to that previously reported to restore normal MeCP2 expression in the mPFC *in vivo* [33] (Fig. 4A). To this end, we designed several sgRNAs specifically targeting exon 3 of the human *MECP2* (Fig. 4B) gene and selected the most efficient sgRNA for follow-up experiments. We discovered that a large number of mutations occurred within the human *MECP2* locus, but none were detected within the counterpart locus of mouse *Mecp2* in an efficiency test of on-target gene editing *in vitro* (Fig. 4C). Moreover, we injected two viruses that packaged SpCas9 (AAV-SpCas9) and sgRNA expression cassettes (AAV-Guide) into the mPFC of transgenic mice, and evaluated the MeCP2 protein levels after 4–6 weeks of viral infection. Our immunofluorescence staining and western blot results showed that the MeCP2 protein levels were decreased by nearly half in the mPFC (Fig. 4D, E). These data demonstrated that our system normalized the MeCP2 levels in specific brain areas *in vivo*.

Next, we explored the hypothesis that normalization of MeCP2 levels in the mPFC is sufficient to reverse the impairment of social recognition. Three groups were used for phenotyping: wild-type mice bilaterally injected with

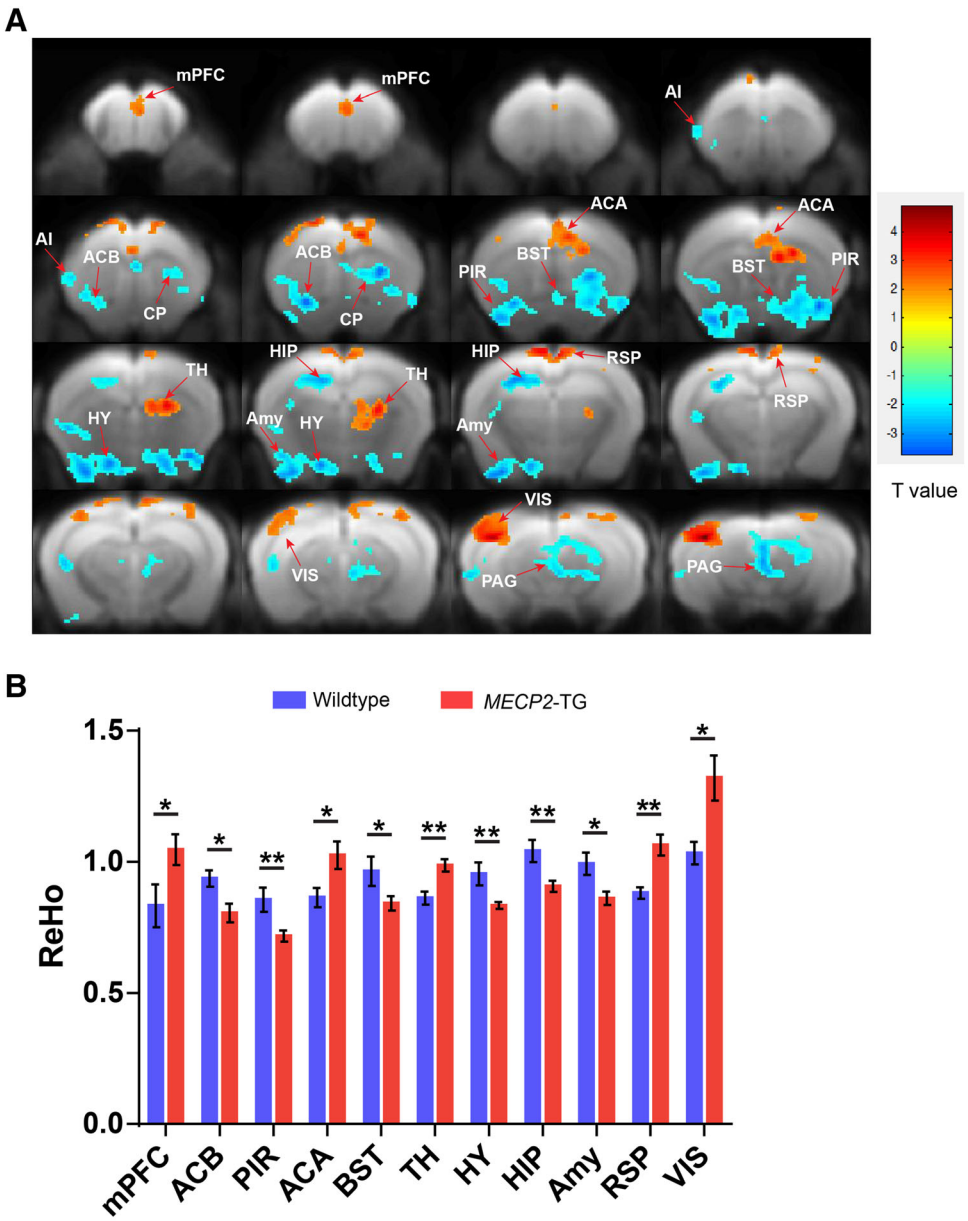


**Fig. 3** Significant ReHo value differences between *MECP2*-TG and wild-type mice in the whole brain resting-state fMRI. **A** Regions manifesting significant ReHo value differences between *MECP2*-TG and wild-type mice (red, *MECP2*-TG > wild-type; blue, wild-type > *MECP2*-TG; color bar represents significance of difference). **B** Quantification of ReHo values in specific brain areas [$n = 10$ for wild-type, $n = 14$ for *MECP2-TG*; data represent the mean ± SEM; $^{*}P < 0.05$, $^{**}P < 0.01$ (two-tailed *t*-test)]. mPFC, medial prefrontal cortex; AI, agranular insular area; ACB, nucleus accumbens; CP, caudoputamen; PIR, piriform area; BST, bed nuclei of the stria terminalis; ACA, anterior cingulate area; TH, thalamus; HY, hypothalamus; HIP, hippocampal region; Amy, amygdala; RSP, retrosplenial area; VIS, visual areas; PAG, periaqueductal gray.

viruses expressing SpCas9 and GFP (Wildtype–CTL), *MECP2*-TG mice bilaterally injected with viruses expressing SpCas9 and GFP (*MECP2*-TG–CTL), and *MECP2*-TG mice bilaterally injected with viruses expressing SpCas9 and sgRNA (*MECP2*-TG–normalized) (Fig. 5A). In our results, the *MECP2*-TG–normalized group indeed spent more time with novel mice than with familiar mice in the three-chamber test, indicating a complete reversal of the social recognition deficit in *MECP2*-TG mice (Fig. 5D). Besides, all three groups showed no side preference and normal social approach behavior, illustrating that viral infection and gene editing manipulation in the mPFC did not impact habituation and social approach behaviors (Fig. 5B, C). Moreover, the reduced locomotor activity, the heightened anxiety-like behaviors, and the fear generalization phenotype were not reversed in the *MECP2*-TG–normalized group (Fig. 5E–J). Together, our results suggested that dysfunction of the mPFC specifically affects social recognition behaviors in *MECP2*-TG mice, and normalization of MeCP2 levels in the mPFC is sufficient to restore the function of the mPFC or mPFC-related circuits, thus completely reversing the social recognition deficit.

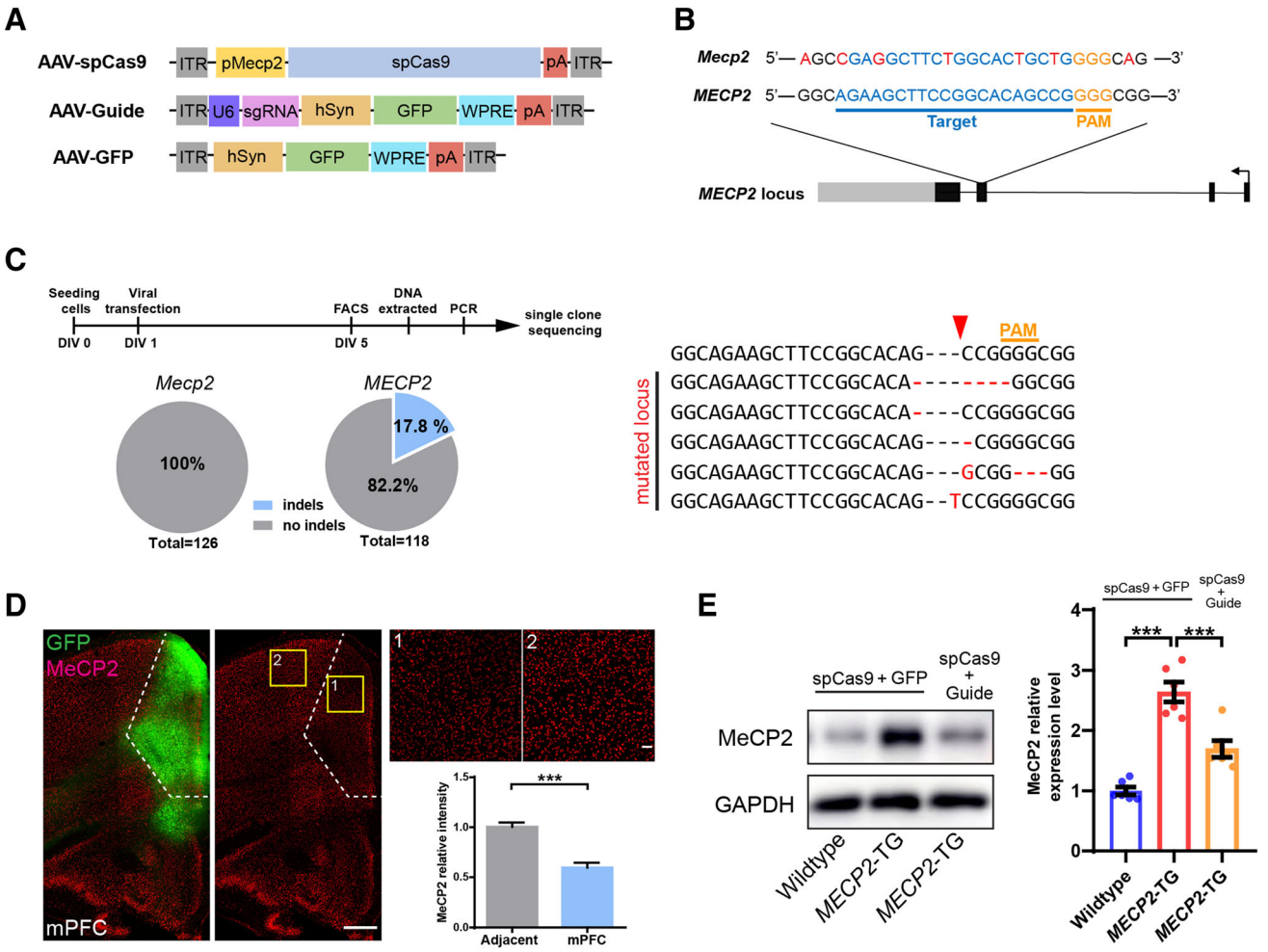


**Fig. 4** Strategy for specific knockout of the human *MECP2* copy in *MECP2* duplication neurons and brain areas of interest in *MECP2* duplication mice. **A** AAV-SpCas9, AAV-Guide, and AAV-GFP expression vectors. **B** SpCas9 target location of the human *MECP2* locus (blue, targeted genomic locus; yellow, PAM (protospacer adjacent motif) sequence; red, mismatched bases between mouse *Mecp2* and the human *MECP2* gene in the targeted locus). **C** Left, protocol for and analysis of on-target gene editing *in vitro*. The efficiency of indel mutations in the *MECP2* locus was ~17.8%, but no indel mutations were detected in the *Mecp2* locus in infected cultured neurons. Right, representative mutation patterns detected by sequencing of the *MECP2* locus (red arrowhead, Cas9 cutting site). **D** Representative images and analysis of MeCP2 expression after CRISPR-Cas9-mediated human *MECP2* knockout in the mPFC *in vivo* (scale bars, 500 µm; $n = 9$ brain slices from 3 mice for each genotype). **E** Western blots and analysis of MeCP2 protein expression 1.5 months after AAV injection [$n = 6$/group; data represent the mean ± SEM; $^{***}P < 0.001$ (two-tailed *t*-test in **D**, and one-way ANOVA followed by Tukey's honest significant difference *post-hoc* correction for multiple comparisons in **E**)].

## Normalization of MeCP2 Levels in the BST Has no Effect on the Behavioral Defects of *MECP2*-TG Mice

In addition to social defects, heightened anxiety is the most prominent behavioral deficit in *MECP2*-TG mice, and a common comorbid condition in patients with *MECP2* duplication syndrome. Many studies have shown that the BST plays a central role in modulating anxiety-related behaviors [34, 35]. Our fMRI data also revealed a significant difference in ReHo values in the BST region between *MECP2*-TG and wild-type mice. We hypothesized that BST dysfunction caused by MeCP2 overexpression leads to a heightened anxiety phenotype in *MECP2*-TG mice. We tested this hypothesis by reducing MeCP2 to normal levels in the BST as we did in the mPFC (Fig. 6A, B). However, neither anxiety-like behaviors in the light–dark box test, nor in the elevated plus maze test were reversed in the *MECP2*-TG–normalized group (Fig. 6G, H). Furthermore, the *MECP2*-TG–normalized group showed no improvement in the reduced locomotor activity in the open field test (Fig. 6F), the impaired social recognition in the three-chamber test (Fig. 6C–E), and the increased freezing behavior in the fear conditioning paradigm (Fig. 6I–K). Given these results, we speculated that the BST is intact in *MECP2*-TG mice, or multiple

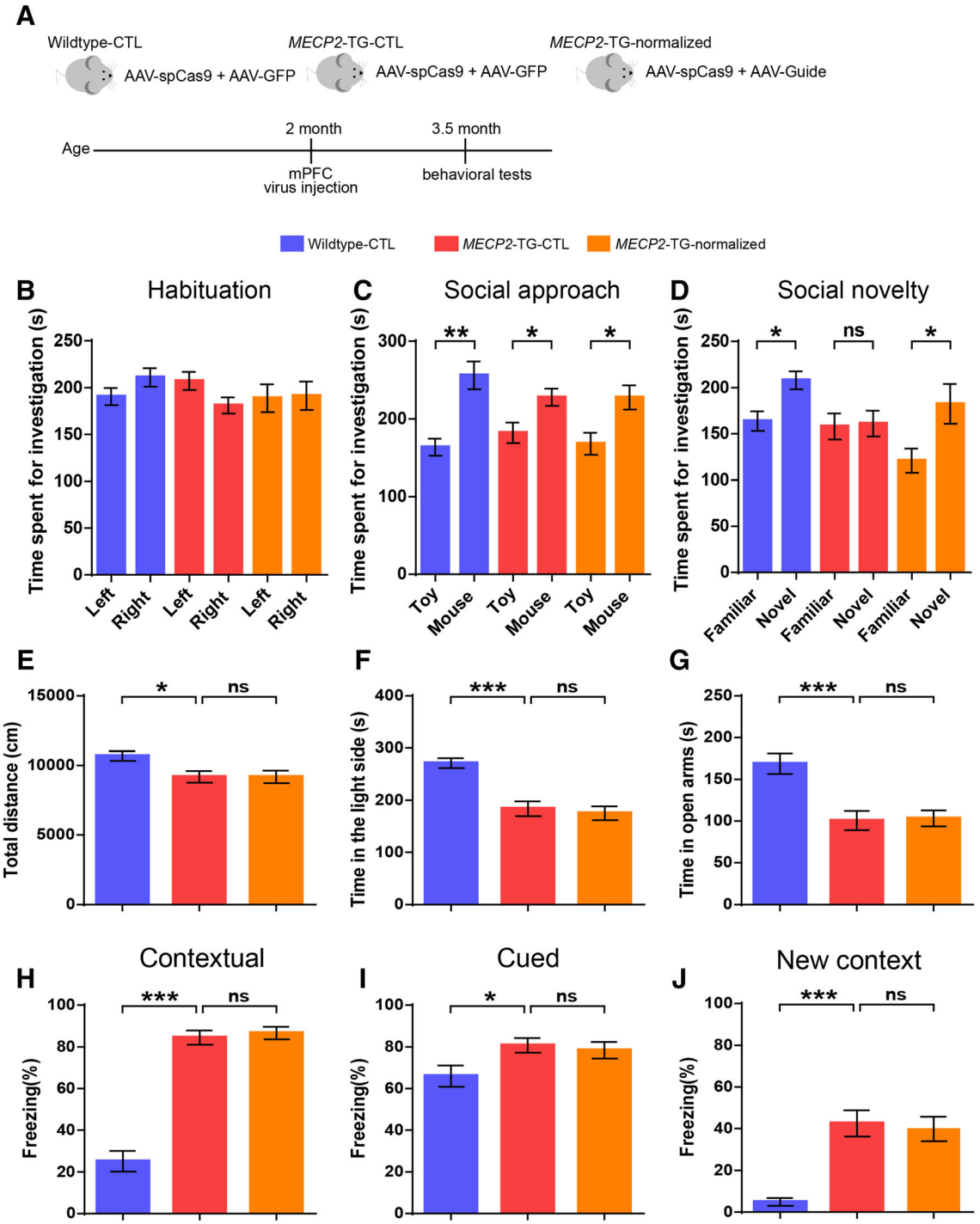


**Fig. 5** Restoration of normal MeCP2 levels in the mPFC reverses the social recognition deficit in adult *MECP2*-TG mice. **A** Schematic of the experimental design. **B–D** Normalizing MeCP2 levels in the mPFC reverses impaired social recognition behavior (**D**) in the three-chamber test. No side preference (**B**) and normal social approach (**C**) were found in the test. **E–J** Normalizing MeCP2 levels in the mPFC of *MECP2*-TG mice did not reverse the decreased locomotor activity in the open field test (**E**), the heightened anxiety-like behaviors in light/dark exploration (**F**) and elevated plus maze (**G**) tests, the percentage freezing when tested on contextual fear memory (**H**) and cued fear memory (**I**), and when presented with a mouse in a new context (**J**). $n = 15$ each for Wildtype–CTL, *MECP2*-TG–CTL, and *MECP2*-TG–normalized; data represent the mean ± SEM; ns, not significant; $^{*}P < 0.05$, $^{**}P < 0.01$, $^{***}P < 0.001$ (two-tailed paired *t*-test in **B–D**, and one-way ANOVA followed by Tukey's honest significant difference *post-hoc* correction for multiple comparisons in **E–J**).

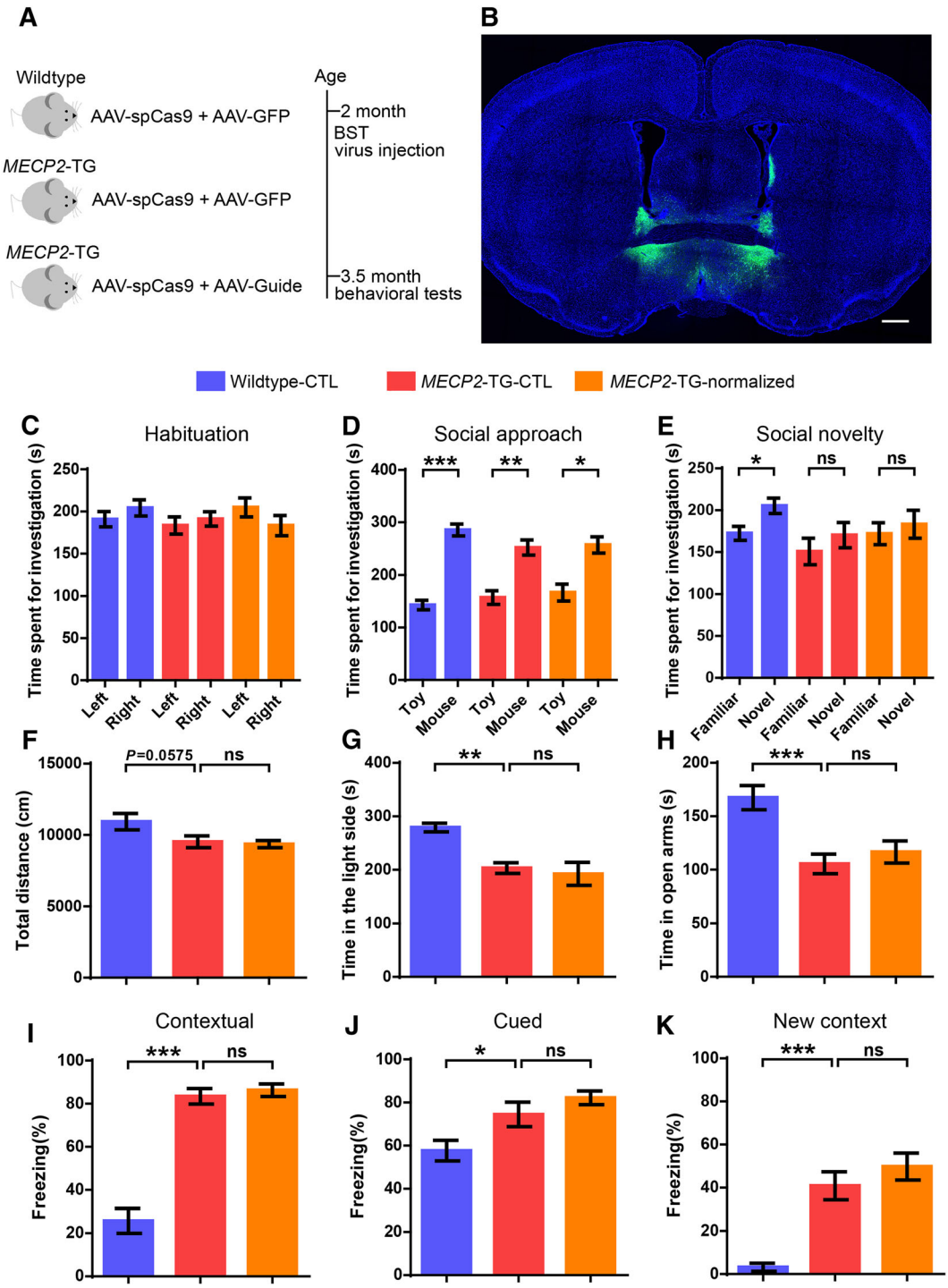


**Fig. 6** Normalization of MeCP2 levels in the BST does not reverse the behavioral defects in *MECP2*-TG mice. **A** Schematic of the experimental design. **B** Representative image of the injection site in the BST (scale bar, 500 μm). **C–K** Normalizing MeCP2 levels in the BST of *MECP2*-TG mice did not reverse the social recognition deficit in the three-chamber test (**C–E**), the decreased locomotor activity in the open field test (**F**), the heightened anxiety-like behaviors in the light/dark exploration (**G**) and elevated plus maze tests (H), and the fear generalization phenotype in the fear conditioning test (**I–K**). $n = 14$ for wild-type–CTL, $n = 14$ for *MECP2*-TG–CTL, $n = 13$ for *MECP2*-TG–normalized. Data represent the mean ± SEM; ns, not significant; $^{*}P < 0.05$, $^{**}P < 0.01$, $^{***}P < 0.001$ (two-tailed paired *t*-test in **C–E**, one-way ANOVA followed by Tukey's honest significant difference *post-hoc* correction for multiple comparisons in **G–K**, and one-way ANOVA followed by Fisher's least significant difference *post-hoc* test in **F**).

brain areas implicated in anxiety are damaged in *MECP2*-TG mice and restoration of MeCP2 levels in the BST is not sufficient to reverse the anxiety-like behaviors.

## Discussion

Our results showed that restoration of normal MeCP2 levels in the mPFC completely reverses the social recognition deficit in adult *MECP2*-TG mice. However, the neural circuit mechanism underlying this deficit in these mice still needs to be investigated. A recent study reported that local gamma oscillation dysfunction in the mPFC is a causative factor for social recognition deficits in a mouse model of autism [21], so local microcircuit dysregulation is probably the main cause of the social defect in *MECP2*-TG mice. Another possibility is that the ability of the mPFC to process social information from upstream brain areas is impaired in *MECP2*-TG mice. Indeed, the ventral tegmental area (VTA), ventral hippocampus (vHIP), HY, and nucleus accumbens are widely reported to project to the mPFC and regulate social behaviors in rodents [34]. Especially, mPFC-projecting neurons in the VTA are mainly dopaminergic, and axons from the VTA innervate broad areas of the mPFC. The latest research shows that dopamine activation in the VTA controls mPFC ensemble activity and oscillations, and oscillation dysfunction in the mPFC is responsible for social recognition impairment in an autistic mouse model [21, 36]. Besides, the vHIP–mPFC projection is hyperactive in the *Mecp2* knockout mouse model of Rett syndrome, which is an another widely-reported autism spectrum disorder mouse model and displays obvious defects in social novelty behavior. And long-term inhibition of mPFC-projecting vHIP neurons in Rett mice rescues the social novelty deficits [37]. These results imply that the VTA–mPFC or vHIP–mPFC projection participates in the regulation of social recognition in rodents. Furthermore, mPFC-mediated top-down control is also implicated in social behaviors. Dysregulation of the input from the mPFC to the basolateral amygdala (BLA) results in impairment of the excitation/inhibition balance in the BLA, which may be the cause of social behavioral defects in autistic model mice [38, 39]. However, whether these neural circuits are damaged and responsible for the behavioral defects in *MECP2*-TG mice remains to be investigated.

We restored normal MeCP2 expression in the BST of adult *MECP2*-TG mice in an attempt to reverse their anxiety-like behaviors, but these behaviors did not improve. Anxiety is an extremely complicated state, and its underlying neural circuit mechanism remains mysterious. A variety of evidence has revealed that neuromodulation systems, the amygdala, vHIP, HY, BST, lateral septal nucleus, and related neural circuits are involved in the regulation of anxiety-like behaviors [35]. It is possible that multiple brain areas or neural circuits involved in anxiety behaviors are damaged in *MECP2*-TG mice, and normalizing the MeCP2 expression only in the BST is not enough to reverse these behaviors. The alternative is that other brain regions contribute more to anxiety than the BST in *MECP2*-TG mice. Our fMRI data showed significant differences in ReHo values between transgenic and wild-type mice in the HY and periaqueductal gray in the midbrain which participate in the regulation of anxiety in rodents. Together, further investigation is needed on the neural mechanisms underlying anxiety in *MECP2*-TG mice.

Another finding that *MECP2*-TG mice showed significant fear generalization deserves further exploration. Many studies indicate that the BLA is the center for regulating fear, and a previous study has demonstrated that BLA-specific deletion of *Mecp2* decreases the freezing level in the cue-dependent fear conditioning test [40]; whether overexpression of MeCP2 in the BLA leads to increased freezing behavior in the fear conditioning test requires further investigation.

## Conclusions

In sum, our study demonstrated that overexpression of MeCP2 in the mPFC is responsible for social deficits. Further studies are still needed to elucidate the neural mechanism underlying the heightened anxiety behaviors and fear generalization phenotype in the transgenic mice. Furthermore, whether specific neural circuit dysfunctions in the transgenic mice are responsible for the behavioral deficits is still to be investigated.

**Acknowledgements** We thank Wen-jing Chen and Kai-Wei Zhang, Institute of Neuroscience, Chinese Academy of Sciences, for assistance with fMRI data collection and advice on the manuscript. And we thank Zhi-Jiang Zhang and Sen Jin, Wuhan Institute of Physics and Mathematics, Chinese Academy of Sciences, for help with the rabies virus tracing experiments. This work was supported by National Natural Science Foundation of China grants (31625013 and 91732302); a Shanghai Brain-Intelligence Project of the Science and Technology Commission of Shanghai Municipality (16JC1420501); and the Strategic Priority Research Program of the Chinese Academy of Sciences (XDBS01060200); Program of Shanghai Academic Research Leader, the Open Large Infrastructure Research of Chinese Academy of Sciences, and the Shanghai Municipal Science and Technology Major Project (2018SHZDZX05); and National Natural Science Foundation of China (81801354).

**Conflict of interest** The authors declare that they have no competing interests.

## References


1. Nan XS, Campoy FJ, Bird A. MeCP2 is a transcriptional repressor with abundant binding sites in genomic chromatin. Cell 1997, 88: 471–481.
2. Chahrour M, Jung SY, Shaw C, Zhou XB, Wong STC, Qin J, *et al*. MeCP2, a key contributor to neurological disease, activates and represses transcription. Science 2008, 320: 1224–1229.
3. Young JI, Hong EP, Castle JC, Crespo-Barreto J, Bowman AB, Rose MF, *et al*. Regulation of RNA splicing by the methylation-dependent transcriptional repressor methyl-CpG binding protein 2. Proc Natl Acad Sci U S A 2005, 102: 17551–17558.
4. Cheng TL, Wang ZZ, Liao QM, Zhu Y, Zhou WH, Xu WQ, *et al*. MeCP2 suppresses nuclear microRNA processing and dendritic growth by regulating the DGCR8/Drosha complex. Devel Cell 2014, 28: 547–560.
5. Cheng TL, Qiu ZL. MeCP2: multifaceted roles in gene regulation and neural development. Neurosci Bull 2014, 30: 601–609.
6. Amir RE, Van den Veyver IB, Wan M, Tran CQ, Francke U, Zoghbi HY. Rett syndrome is caused by mutations in X-linked MECP2, encoding methyl-CpG-binding protein 2. Nat Genet 1999, 23: 185–188.
7. Chahrour M, Zoghbi HY. The story of Rett syndrome: From clinic to neurobiology. Neuron 2007, 56: 422–437.
8. Van Esch H, Bauters M, Ignatius J, Jansen M, Raynaud M, Hollanders K, *et al*. Duplication of the MECP2 region is a frequent cause of severe mental retardation and progressive neurological symptoms in males. Am J Hum Genet 2005, 77: 442–453.
9. Ramocki MB, Peters SU, Tavyev YJ, Zhang F, Carvalho CMB, Schaaf CP, *et al*. Autism and other neuropsychiatric symptoms are prevalent in individuals with MECP2 duplication syndrome. Ann Neurol 2009, 66: 771–782.
10. Ramocki MB, Tavyev YJ, Peters SU. The MECP2 duplication syndrome. Am J Med Genet Part A 2010, 152A: 1079–1088.
11. Collins AL, Levenson JM, Vilaythong AP, Richman R, Armstrong DL, Noebels JL, *et al*. Mild overexpression of MeCP2 causes a progressive neurological disorder in mice. Hum Mol Genet 2004, 13: 2679–2689.
12. Samaco RC, Mandel-Brehm C, McGraw CM, Shaw CA, McGill BE, Zoghbi HY. Crh and Oprm1 mediate anxiety-related behavior and social approach in a mouse model of MECP2 duplication syndrome. Nat Genet 2012, 44: 206–211.
13. del Gaudio D, Fang P, Scaglia F, Ward PA, Craigen WJ, Glaze DG, *et al*. Increased MECP2 gene copy number as the result of genomic duplication in neurodevelopmentally delayed males. Genet Med 2006, 8: 784–792.
14. Heckman LD, Chahrour MH, Zoghbi HY. Rett-causing mutations reveal two domains critical for MeCP2 function and for toxicity in MECP2 duplication syndrome mice. Elife 2014, 3.
15. Jiang MH, Ash RT, Baker SA, Suter B, Ferguson A, Park J, *et al*. Dendritic arborization and spine dynamics are abnormal in the mouse model of MECP2 duplication syndrome. J Neurosci 2013, 33: 19518–19533.
16. Nageshappa S, Carromeu C, Trujillo CA, Mesci P, Espuny-Camacho I, Pasciuto E, *et al*. Altered neuronal network and rescue in a human MECP2 duplication model. Molecular Psychiatry 2016, 21: 178–188.
17. Chao HT, Zoghbi HY, Rosenmund C. MeCP2 controls excitatory synaptic strength by regulating glutamatergic synapse number. Neuron 2007, 56: 58–65.
18. Lu H, Ash RT, He LJ, Kee SE, Wang W, Yu DH, *et al*. Loss and gain of MeCP2 cause similar hippocampal circuit dysfunction that is rescued by deep brain stimulation in a Rett syndrome mouse model. Neuron 2016, 91: 739–747.
19. Sztainberg Y, Chen HM, Swann JW, Hao S, Tang B, Wu ZY, *et al*. Reversal of phenotypes in MECP2 duplication mice using genetic rescue or antisense oligos. Nature 2015, 528: 123–126.
20. Cook MN, Williams RW, Flaherty L. Anxiety-related behaviors in the elevated zero-maze are affected by genetic factors and retinal degeneration. Behav Neurosci 2001, 115: 468–476.
21. Cao W, Lin S, Xia QQ, Du YL, Yang Q, Zhang MY, *et al*. Gamma oscillation dysfunction in mPFC leads to social deficits in Neuroligin 3 R451C knockin mice. Neuron 2018, 97: 1253–1260.
22. Li RP, Liu XP, Sidabras JW, Paulson ES, Jesmanowicz A, Nencka AS, *et al*. Restoring susceptibility induced MRI signal loss in rat brain at 9.4 T: a step towards whole brain functional connectivity imaging. PLoS One 2015, 10.
23. Dorr AE, Lerch JP, Spring S, Kabani N, Henkelman RM. High resolution three-dimensional brain atlas using an average magnetic resonance image of 40 adult C57Bl/6 J mice. Neuroimage 2008, 42: 60–69.
24. Avants BB, Tustison NJ, Song G, Cook PA, Klein A, Gee JC. A reproducible evaluation of ANTs similarity metric performance in brain image registration. Neuroimage 2011, 54: 2033–2044.
25. Zou QH, Zhu CZ, Yang YH, Zuo XN, Long XY, Cao QJ, *et al*. An improved approach to detection of amplitude of low-frequency fluctuation (ALFF) for resting-state fMRI: Fractional ALFF. J Neurosci Methods 2008, 172: 137–141.
26. Fyffe SL, Neul JL, Samaco RC, Chao HT, Ben-Shachar S, Moretti P, *et al*. Deletion of Mecp2 in Sim1-expressing neurons reveals a critical role for MeCP2 in feeding behavior, aggression, and the response to stress. Neuron 2008, 59: 947–958.
27. Ito-Ishida A, Ure K, Chen H, Swann JW, Zoghbi HY. Loss of MeCP2 in parvalbumin-and somatostatin-expressing neurons in mice leads to distinct rett syndrome-like phenotypes. Neuron 2015, 88: 651–658.
28. Samaco RC, Mandel-Brehm C, Chao HT, Ward CS, Fyffe-Maricich SL, Ren J, *et al*. Loss of MeCP2 in aminergic neurons causes cell-autonomous defects in neurotransmitter synthesis and specific behavioral abnormalities. Proc Natl Acad Sci U S A 2009, 106: 21966–21971.
29. Finlay JM, Dunham GA, Isherwood AM, Newton CJ, Nguyen TV, Reppar PC, *et al*. Effects of prefrontal cortex and hippocampal NMDA NR1-subunit deletion on complex cognitive and social behaviors. Brain Res 2015, 1600: 70–83.
30. Liang B, Zhang LF, Barbera G, Fang WT, Zhang J, Chen XC, *et al*. Distinct and dynamic ON and OFF neural ensembles in the prefrontal cortex code social exploration. Neuron 2018, 100: 700–714.e9.
31. Niu B, Liu PP, Shen MJ, Liu C, Wang L, Wang FF, *et al*. GRK5 regulates social behavior via suppression of mTORC1 signaling in medial prefrontal cortex. Cereb Cortex 2018, 28: 421–432.
32. Tan Y, Singhal SM, Harden SW, Cahill KM, Nguyen DTM, Colon-Perez LM, *et al*. Oxytocin receptors are expressed by glutamatergic prefrontal cortical neurons that selectively modulate social recognition. J Neurosci 2019, 39: 3249–3263.
33. Swiech L, Heidenreich M, Banerjee A, Habib N, Li YQ, Trombetta J, *et al*. *In vivo* interrogation of gene function in the mammalian brain using CRISPR-Cas9. Nat Biotechnol 2015, 33: U102–U286.
34. Allsop SA, Vander Weele CM, Wichmann R, Tye KM. Optogenetic insights on the relationship between anxiety-related behaviors and social deficits. Front Behav Neurosci 2014, 8.
35. Tovote P, Fadok JP, Luthi A. Neuronal circuits for fear and anxiety. Nat Rev Neurosci 2015, 16: 317–331.
36. Lohani S, Martig AK, Deisseroth K, Witten IB, Moghaddam B. Dopamine modulation of prefrontal cortex activity is manifold and operates at multiple temporal and spatial scales. Cell Rep 2019, 27: 99–114.e6.

37. Phillips ML, Robinson HA, Pozzo-Miller L. Ventral hippocampal projections to the medial prefrontal cortex regulate social memory. Elife 2019, 8.
38. Li Y, Missig G, Finger BC, Landino SM, Alexander AJ, Mokler EL, *et al*. Maternal and early postnatal immune activation produce dissociable effects on neurotransmission in mPFC-amygdala circuits. J Neurosci 2018, 38: 3358–3372.
39. Huang WC, Chen YJ, Page DT. Hyperconnectivity of prefrontal cortex to amygdala projections in a mouse model of macrocephaly/autism syndrome. Nat Commun 2016, 7.
40. Adachi M, Autry AE, Covington HE, Monteggia LM. MeCP2-mediated transcription repression in the basolateral amygdala may underlie heightened anxiety in a mouse model of rett syndrome. J Neurosci 2009, 29: 4218–4227.